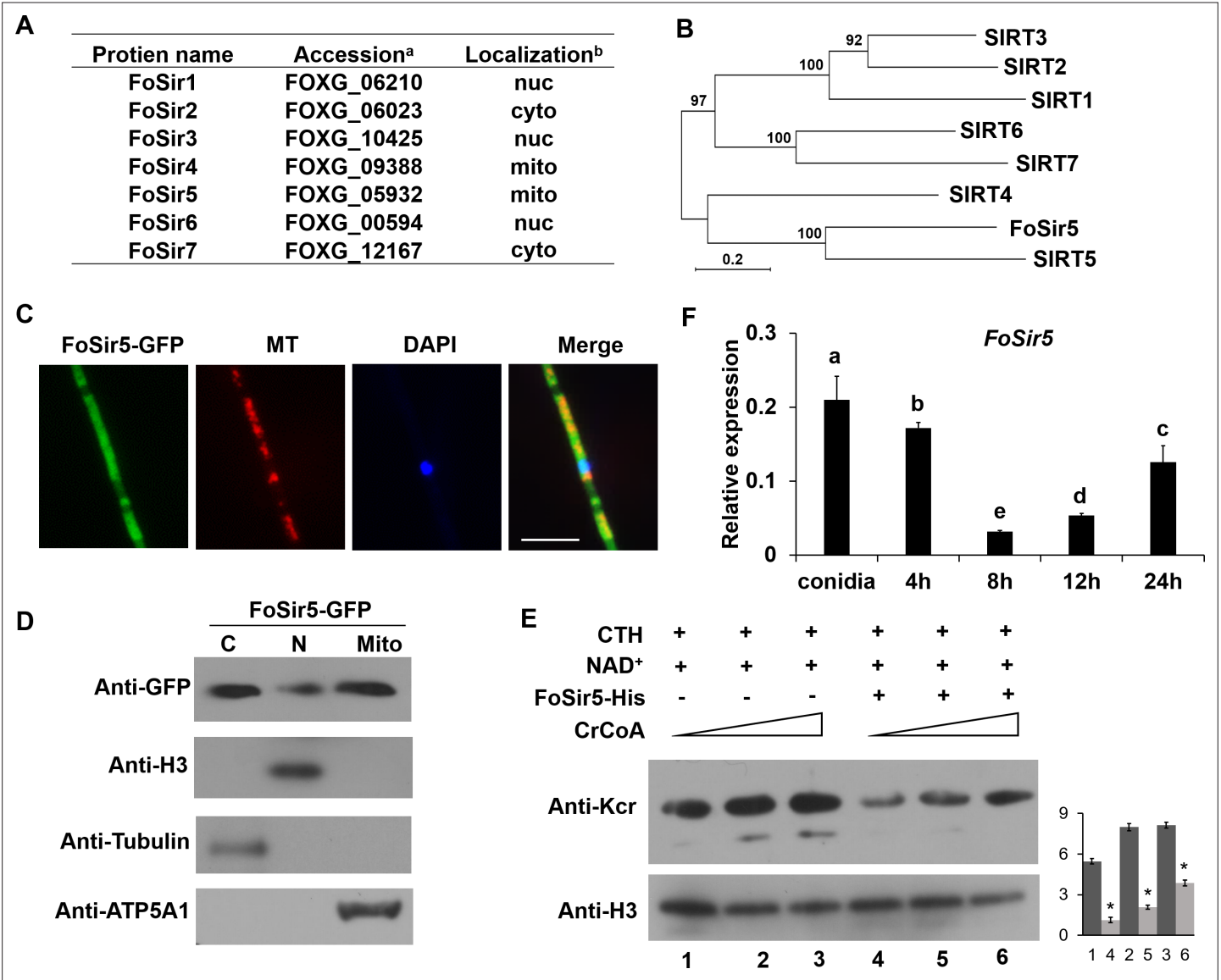


---

## Figures and figure supplements

The decrotonylase FoSir5 facilitates mitochondrial metabolic state switching in conidial germination of *Fusarium oxysporum*

**Ning Zhang et al**



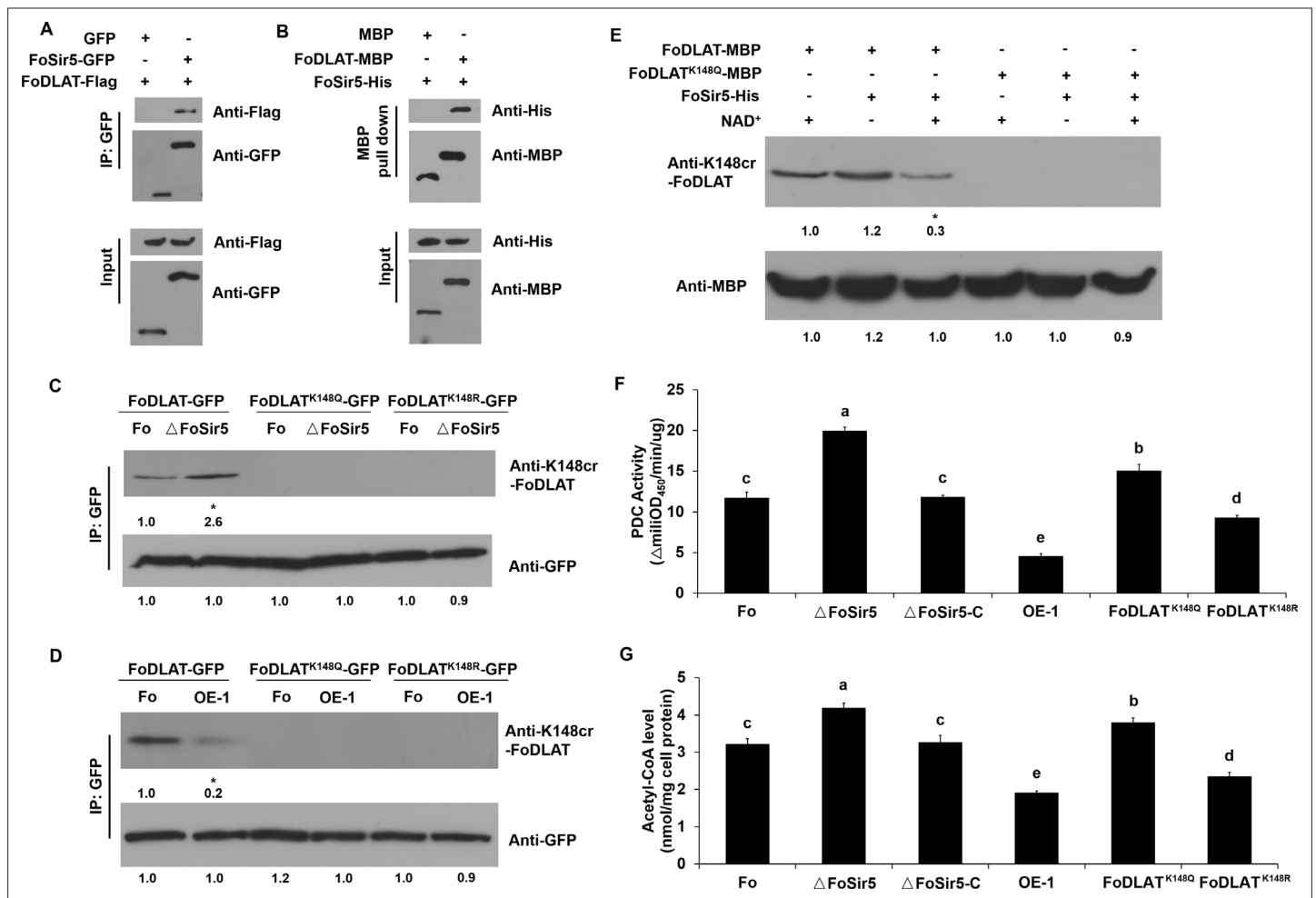


**Figure 2.** FoSir5 deacetylates FoDLAT, the E2 component of *Fusarium oxysporum* pyruvate decarboxylase complex, with regulatory consequence. (A) Co-IP assays reveal physical interaction of FoSir5-GFP and FoDLAT-Flag. Western blot analysis of cell extracts from transformants co-expressing FoDLAT-Flag with GFP or FoSir5-GFP and elution from anti-GFP agarose. The fusion proteins were detected with anti-Flag or anti-GFP antibody. (B) In vitro pull-down assays to detect FoSir5-His with MBP or the FoDLAT-MBP fusion protein. FoDLAT-MBP was used as bait to pull down the FoSir5-His protein from the induced cell extracts. The MBP protein was assayed as a negative control. Input and bound forms of the pull-down fractions were detected with anti-His or anti-MBP antibody. (C–D) The K148 crotonylation (anti-K148cr-FoDLAT, top panel) and amount (anti-GFP, bottom panel) of FoDLAT-GFP and its mutant isoforms in the  $\Delta$ FoSir5 (C) and OE-1 strain (D). Proteins were immunoprecipitated with anti-GFP antibody agarose beads and analyzed by anti-K148cr-FoDLAT or anti-GFP antibody. Representative gels are shown from experiments carried out at least twice. Numbers below the blots represent the relative abundance of K148-crotonylated FoDLAT. Anti-GFP immunoblotting was used to show equal loading. (E) FoSir5 directly deacetylates FoDLAT in vitro. Purified FoDLAT protein or its K148Q isoform (50 ng) were incubated with or without 50 ng of purified FoSir5 in the absence or presence of 5 mM NAD<sup>+</sup> and then analyzed by immunoblotting using anti-K148cr-FoDLAT or anti-His antibody. Each gel shown is representative of two experiments. Numbers below the blots represent the relative abundance of K148-crotonylated FoDLAT. Anti-MBP immunoblotting was used to show equal loading. (F–G) FoSir5 and K148 mutant FoDLAT affected pyruvate dehydrogenase complex (PDC) activity (F) and acetyl-CoA production (G) in *F. oxysporum*. PDC activity and acetyl-CoA production were determined in germinating conidia at 8 hr. The presence of different letters above the mean values of three replicates indicates a significant difference between different strains ( $p < 0.05$ , ANOVA).

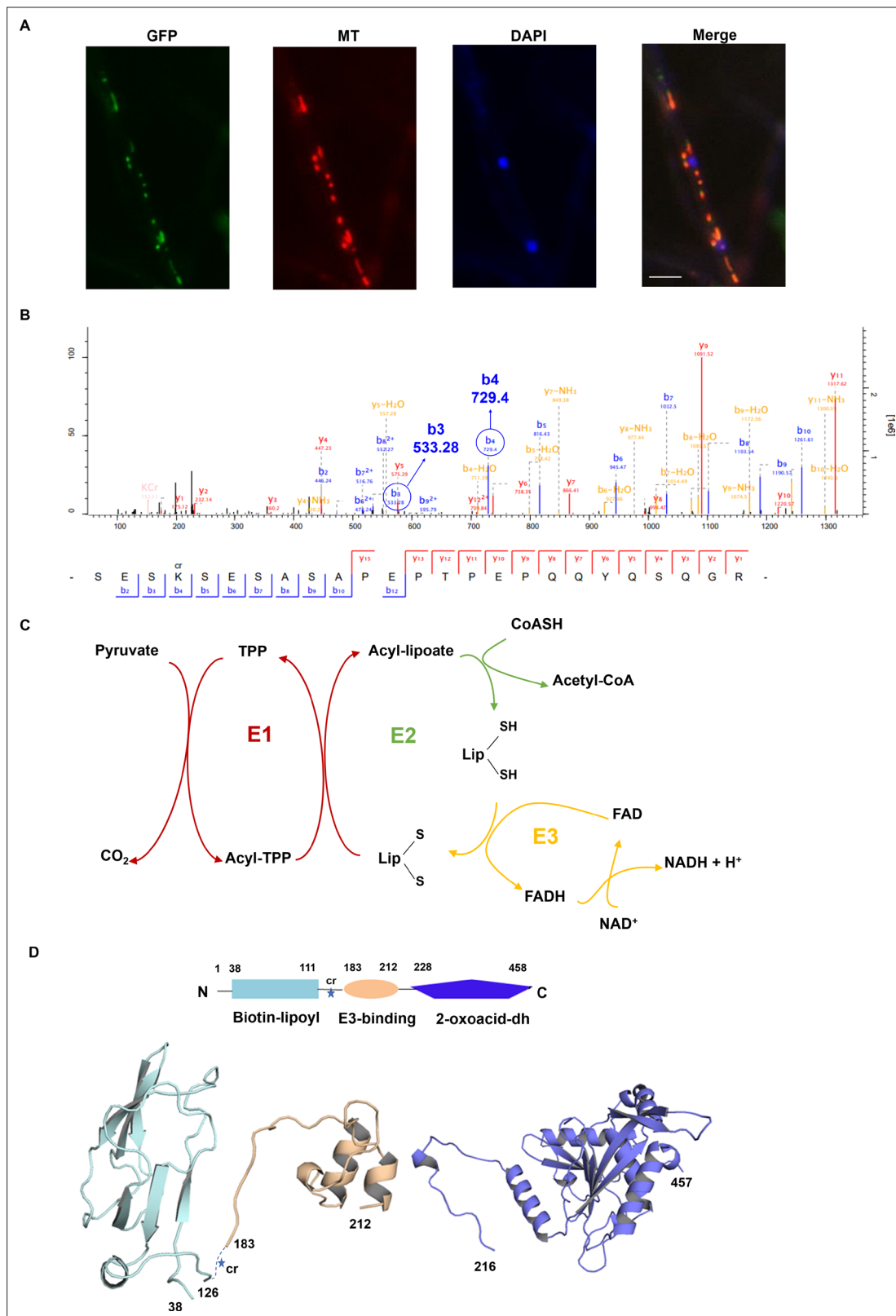


**Figure 2—figure supplement 1.** Interpretation of the subcellular location, Kcr site, and protein structure of FoDLAT. **(A)** Fluorescence microscopy analysis of the FoDLAT-GFP localization along with MitoTracker Red (MT) and DAPI. Scale bars = 10  $\mu$ m. **(B)** Annotation of representative tandem mass spectra from trypsin-digested FoDLAT-GFP in *Fusarium oxysporum* depicting K148 crotonylation. **(C)** Schematic of the chemical transformations catalyzed by the E1 and E3 subunits of pyruvate dehydrogenase. **(D)** Homology models of the FoDLAT domains predicted by the PHYRE fold server. FoDLAT domain boundary is defined using Motif program to against Pfam, NCBI-CDD database. The star indicates the K148 crotonylation site.



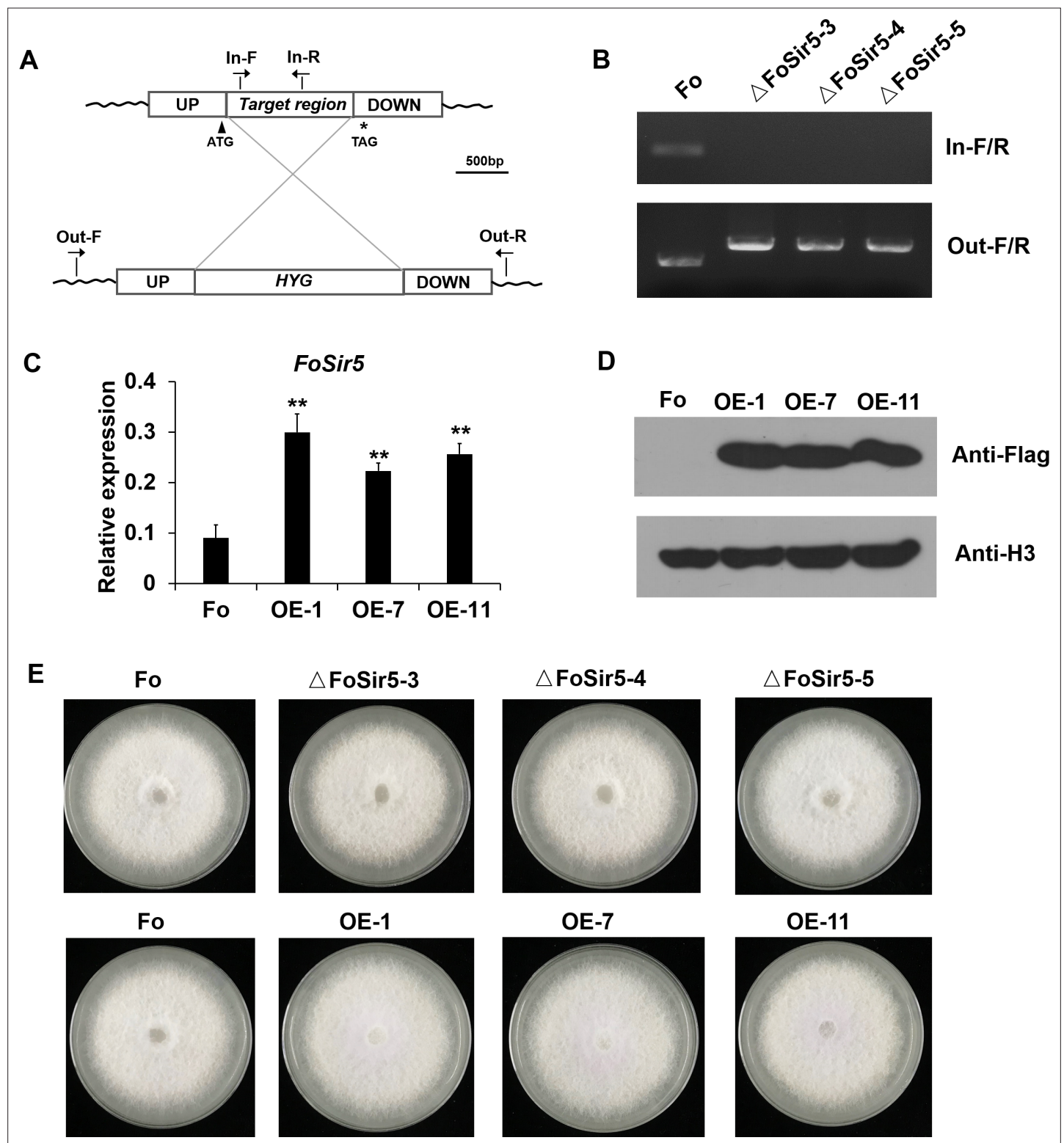


**Figure 2—figure supplement 2.** Generation of targeted *FoSir5* gene deletion mutants and overexpression transformants. (A) Schematic representation of the targeted deletion of *FoSir5*. (B) PCR analysis of targeted deletion in the  $\Delta FoSir5$  strains. Genomic DNA was analyzed by PCR with the primer pairs indicated in panel (A). (C–D) Real-time (RT)-PCR (C) and Western blotting (WB) (D) analysis of the *FoSir5*-Flag-overexpression transformants. Data of RT-PCR are the means  $\pm$  SDs ( $n = 3$ ); \*\* $p < 0.05$  by unpaired two-tailed t-test. (E) Mycelial growth of the indicated strains on PDA plates after 3 days of cultivation.

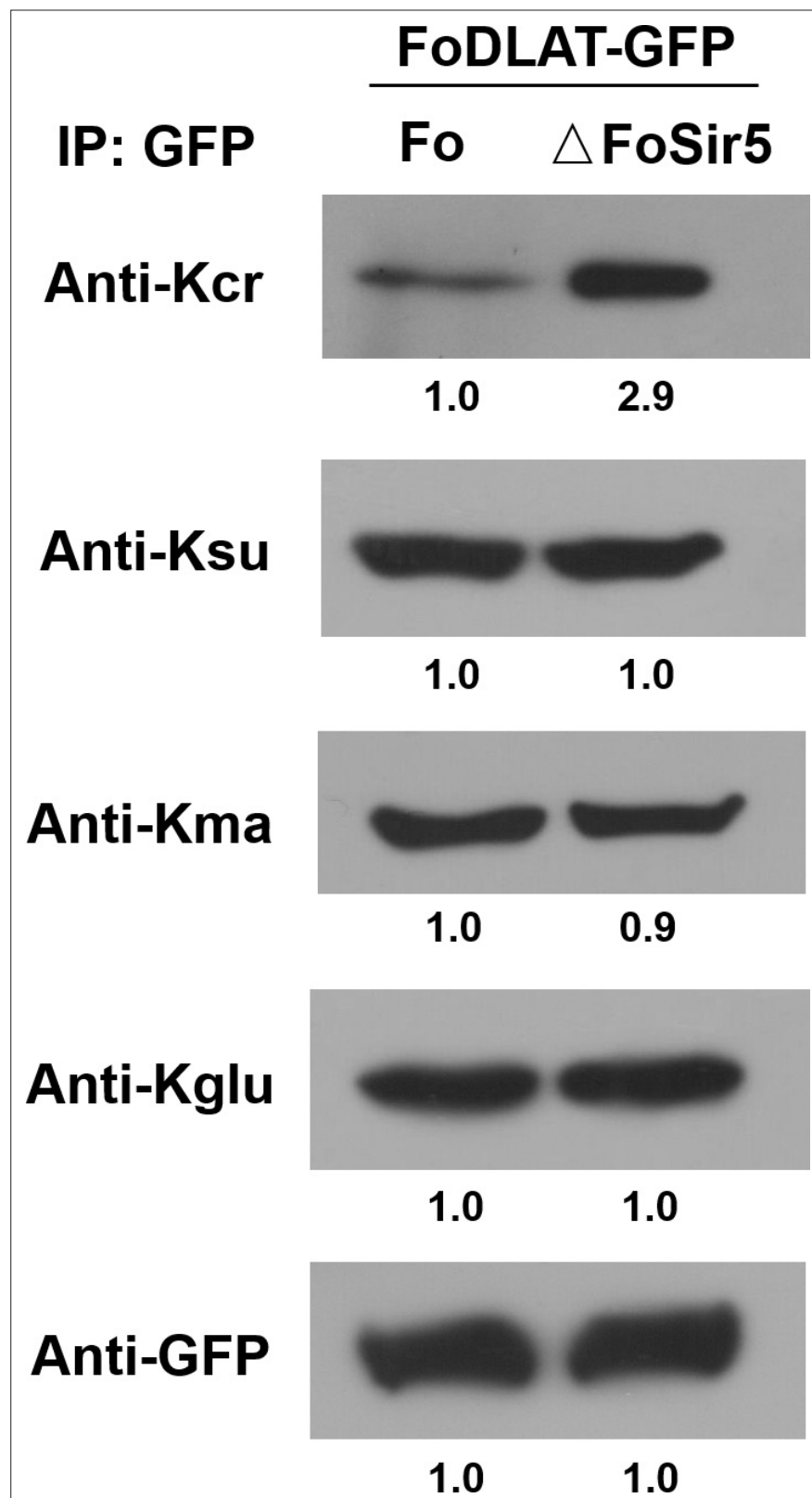


**Figure 2—figure supplement 3.** Detection of crotonylation, succinylation, malonylation, and glutarylation on FoDLAT protein in  $\Delta$ FoSir5 compared with Fo. Proteins were immunoprecipitated with anti-GFP antibody agarose beads and analyzed by Western blot using the indicated antibodies. Representative gels are shown from experiments carried out at least twice. Anti-GFP immunoblotting was used to show equal loading.

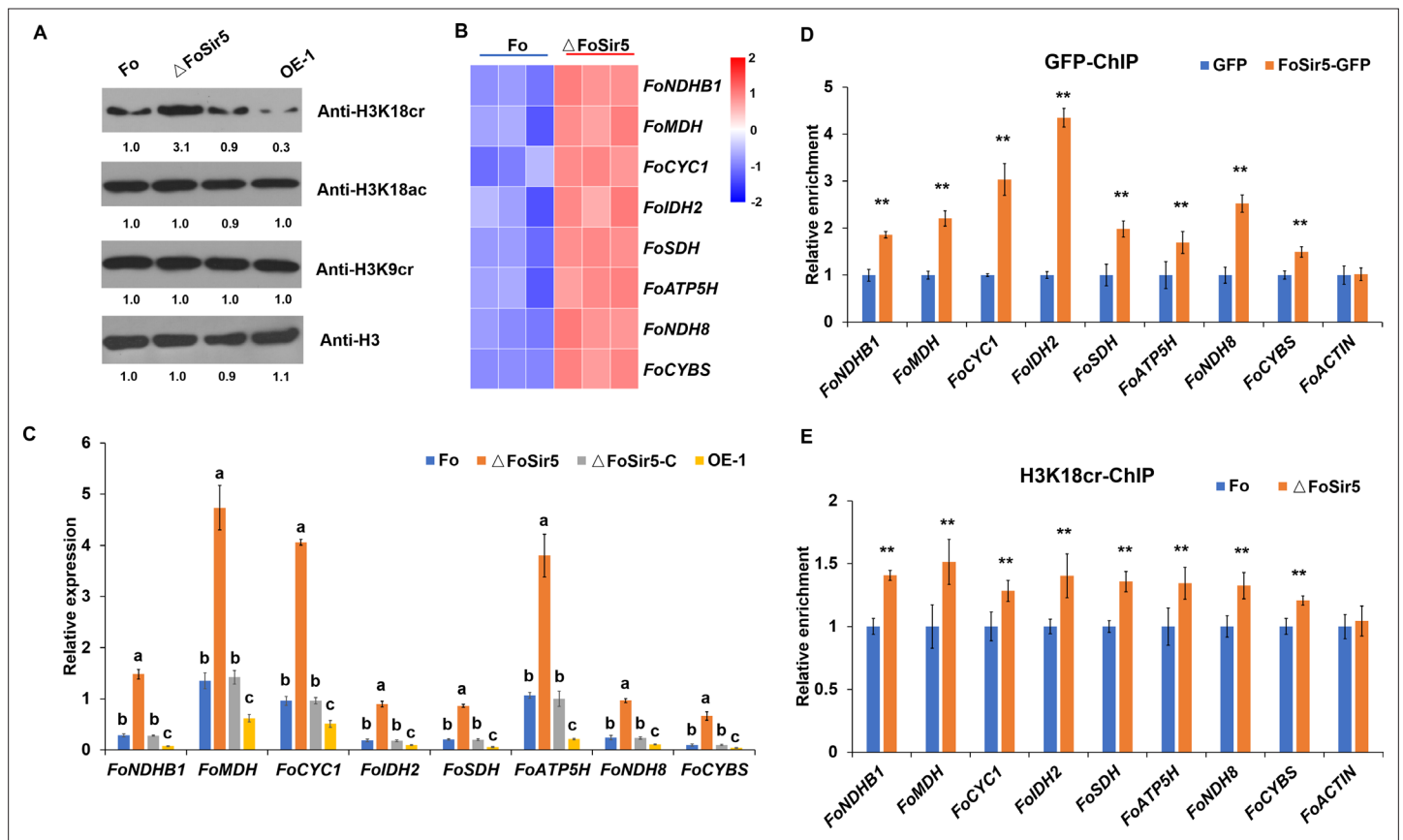


**Figure 3.** The downregulation of H3K18 crotonylation by *FoSir5* and transcriptional repression of aerobic respiration-related genes. **(A)** Western blot analysis showed the effect of *FoSir5* on histone H3K18 crotonylation and acetylation, and histone H3K9 crotonylation using the indicated antibodies. Numbers below the blots represent the relative abundance of different modifications. Anti-H3 immunoblotting was used to show equal loading. **(B)** RNA-seq analysis of eight upregulated genes involved in aerobic respiration including *NDHB1* (NADH-quinone oxidoreductase chain B 1), *MDH* (malate dehydrogenase), *CYC1* (cytochrome C1), *IDH2* (isocitrate dehydrogenase subunit 2), *SDH* (succinate dehydrogenase), *ATP5H* (ATP synthase D chain), *NDH8* (NADH dehydrogenase iron-sulfur protein 8), and *CYBS* (succinate dehydrogenase cytochrome b small subunit). Differential expression in three biological replicates illustrated using a heat map with colored squares indicating the range of expression referred to as the FPKM value. **(C)** qRT-PCR validation of aerobic respiration-related genes in the indicated strains. The letters above the mean values of three replicates indicate significant differences between different strains (p < 0.05, ANOVA). **(D–E)** Relative enrichment of the immunoprecipitated promoter regions in aerobic respiration-related genes determined using anti-GFP antibody in the *FoSir5*-GFP strain and *Fo* strain containing GFP alone **(D)** or using anti-H3K18cr antibody in the *Fo* and  $\Delta$ *FoSir5* mutant strains **(E)**. The fold enrichment was normalized to the input and internal control gene ( *$\beta$ -tubulin*). Data are the means  $\pm$  SDs (n = 3); \*\*p < 0.05 by unpaired two-tailed t-test.

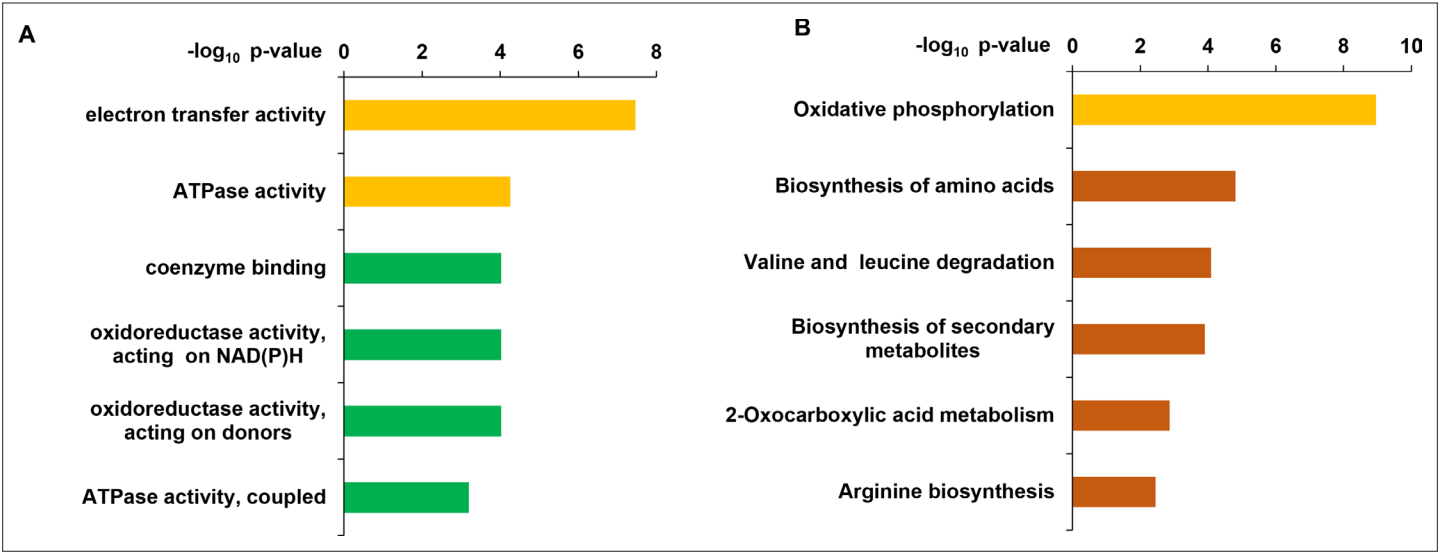


**Figure 3—figure supplement 1.** Distribution of functional classification of Gene Ontology (GO) (A) and KEGG pathway (B) of the upregulated genes in  $\Delta$ FoSir5 compared with Fo. Histograms indicate p-values of the enriched functional categories.

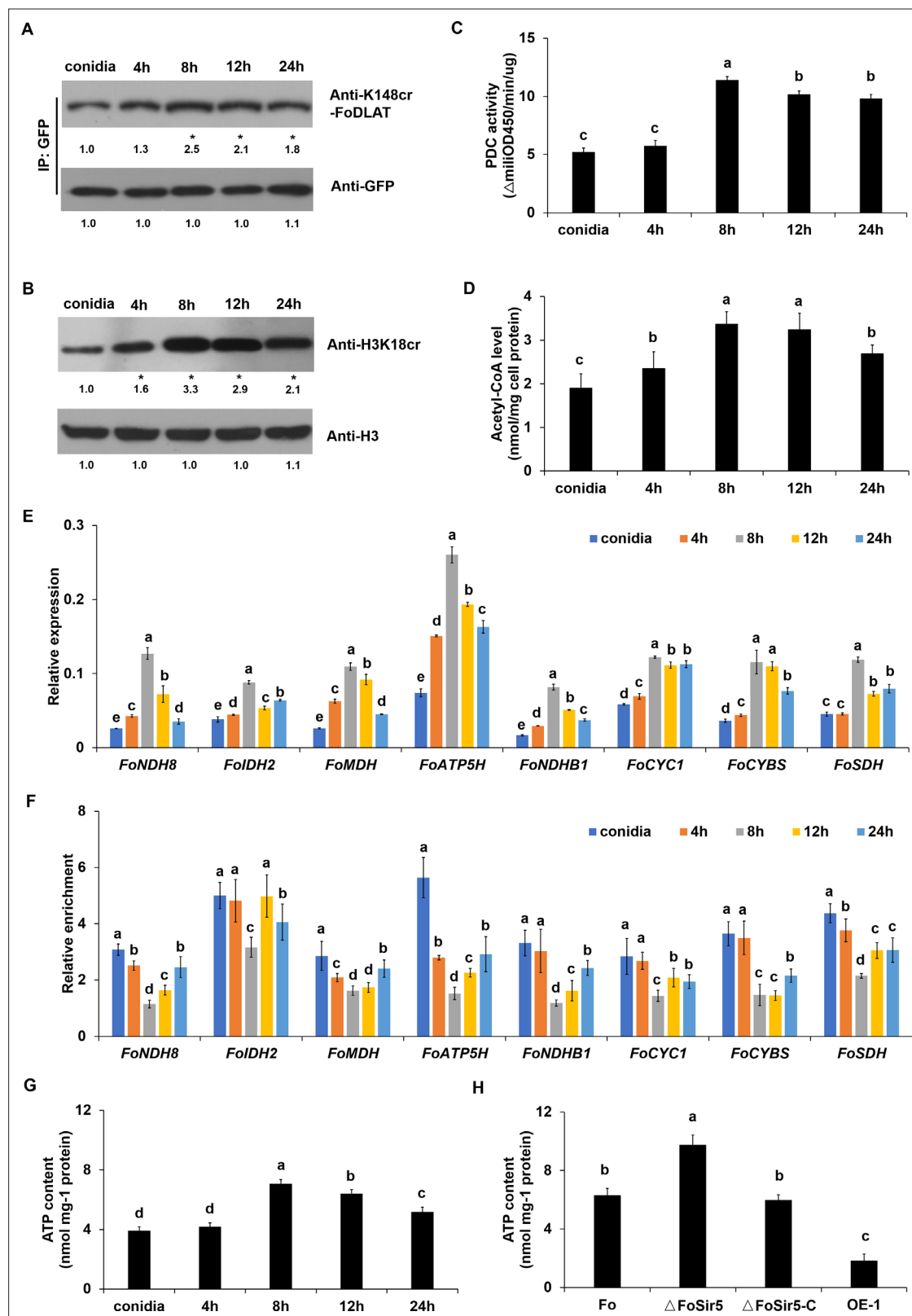


**Figure 4.** FoSir5 affects ATP production during germination in *Fusarium oxysporum*. (A–B) Western blot analysis showed the dynamic changes of FoDLAT K148 (A) and histone H3K18 (B) crotonylation during germination using the indicated antibodies. Numbers below the blots represent the relative abundance of FoDLAT-K148cr or H3K18cr. Anti-GFP or anti-H3 immunoblotting was used to show equal loading, respectively. (C–D) Pyruvate dehydrogenase complex (PDC) activity (C) and acetyl-CoA production (D) in *F. oxysporum* during germination were determined. (E) Expression profile

Figure 4 continued on next page

## Figure 4 continued

of the aerobic respiration-related genes during the germination process. **(F)** Relative enrichment of the immunoprecipitated promoter regions in aerobic respiration-related genes during germination determined using anti-GFP antibody in the FoSir5-GFP strain driven by the native promoter. The fold enrichment was normalized to the input and internal control gene (*β-tubulin*). **(G)** ATP content of *F. oxysporum* during germination. **(H)** Effect of FoSir5 on the ATP content of the indicated strains, as determined in germinating conidia at 8 hr post incubation (h.p.r.). The presence of different letters **(A–H)** above the mean values of three replicates indicates a significant difference between different samples ( $p < 0.05$ , ANOVA).

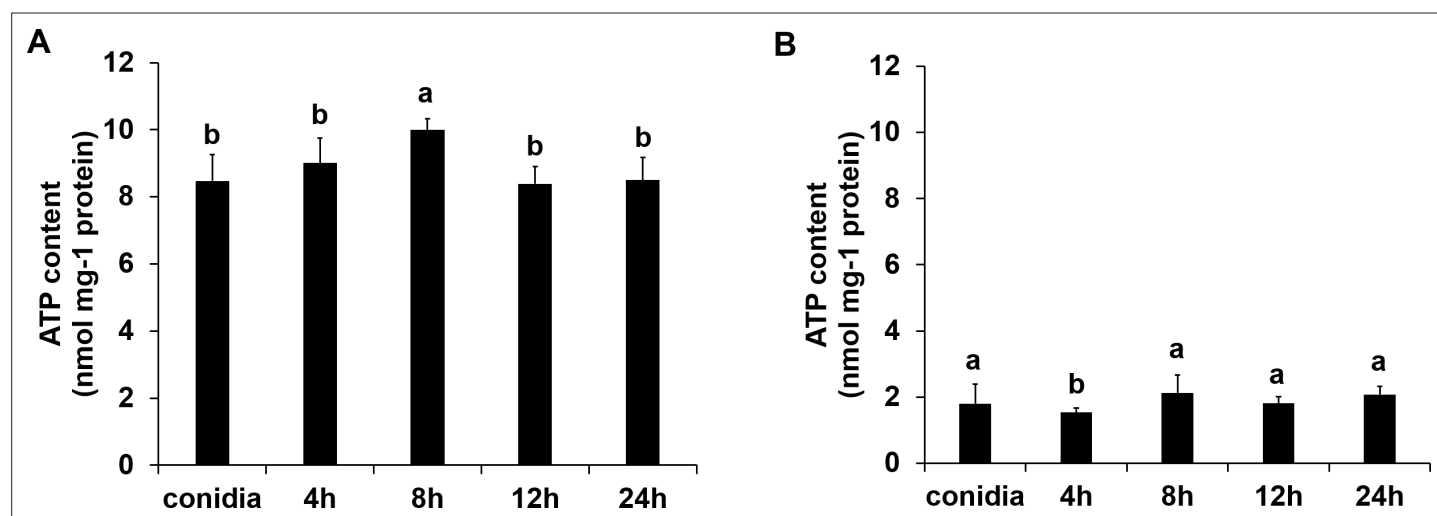


**Figure 4—figure supplement 1.** The ATP content of  $\Delta$ FoSir5 mutant (A) and OE-1 strain (B) during germinating process. The presence of different letters above the mean values of three replicates indicates a significant difference between different samples ( $p < 0.05$ , ANOVA).

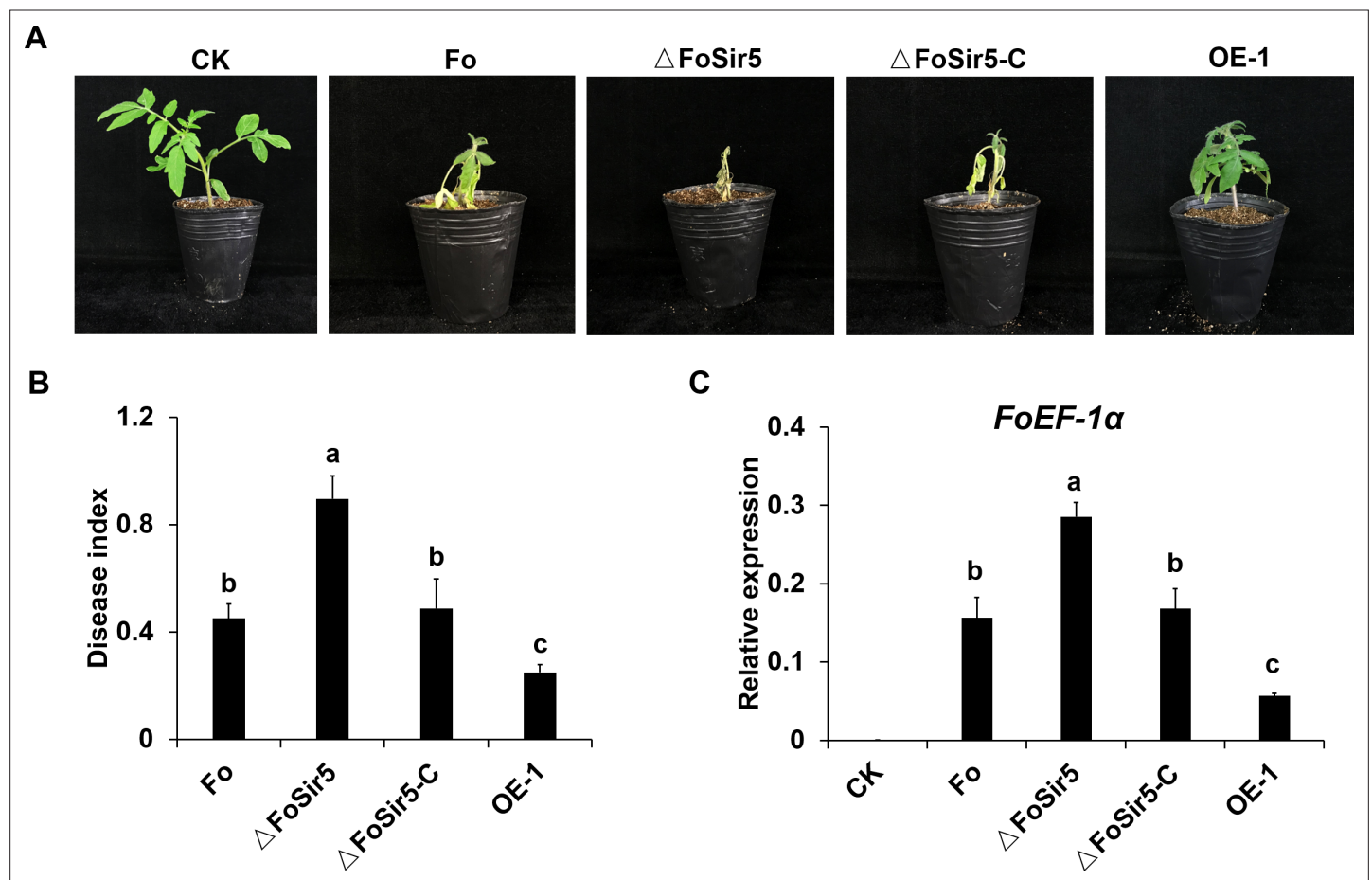


**Figure 4—figure supplement 2.** Impact of FoSir5 on the virulence of *Fusarium oxysporum*.

(A) Pathogenicity of the indicated strains in tomato after 8 days of incubation. (B) Quantification of the disease indexes of the indicated strains. (C) Quantitative real-time PCR (qRT-PCR) analysis of *F. oxysporum* *EF-1 $\alpha$*  transcript levels in tomato plants harvested 14 days after infection with the indicated strains. The expression of tomato *RCE1*, a constitutively expressed gene, was used as a control for the use of equal amounts of RNA for RT-PCR. The letters (B and C) above the mean values of three replicates indicate significant differences between different strains ( $p < 0.05$ , ANOVA).



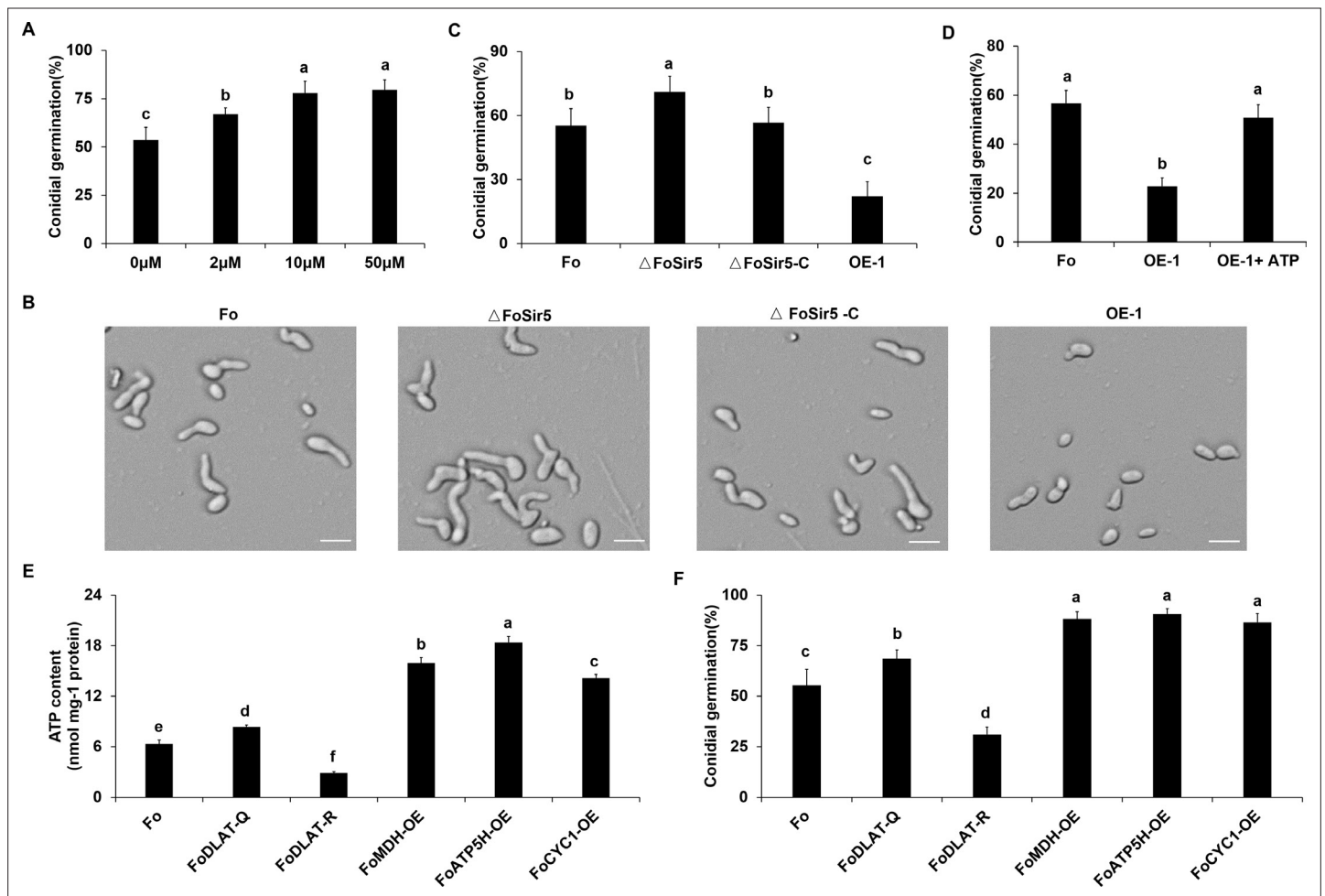


**Figure 5.** FoSir5 modulates conidial germination through affecting ATP synthesis. (A) Quantification of the conidial germination of *Fusarium oxysporum* in PDB supplied with different concentrations of exogenous ATP at 8 h.p.r. (B) Conidial germination of the indicated strains in PDB on glass slides at 8 h.p.r. Representative images from three or more independent experiments, all of which had similar results. Scale bars = 30 μm. (C) Quantification of the conidial germination of the indicated strains in PDB on glass slides at 8 h.p.r. (D) Quantification of the conidial germination of the OE-1 strain with or without treatment with exogenous ATP at 8 h.p.r. (E–F) Effect of FoDLAT -K148Q/R mutations or overexpression of key genes of aerobic respiration on ATP production (E) and conidial germination (F) in *F. oxysporum*. The ATP content and germinating rate were determined at 8 h.p.r. The letters (A–F) above the mean values of three replicates indicate significant differences between different strains ( $p < 0.05$ , ANOVA).

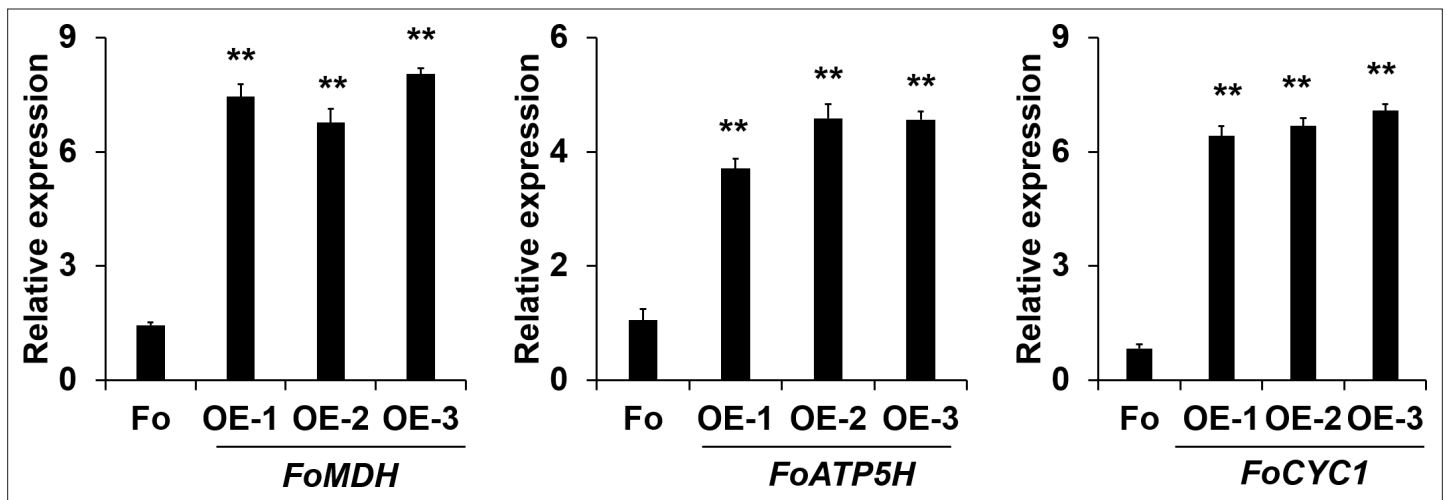


**Figure 5—figure supplement 1.** Real-time PCR (RT-PCR) analysis of *FoMDH*-, *FoATP5H*-, and *FoCYC1*-overexpressing transformants. Data are the means  $\pm$  SDs ( $n = 3$ ); \*\* $p < 0.05$  by unpaired two-tailed t-test.

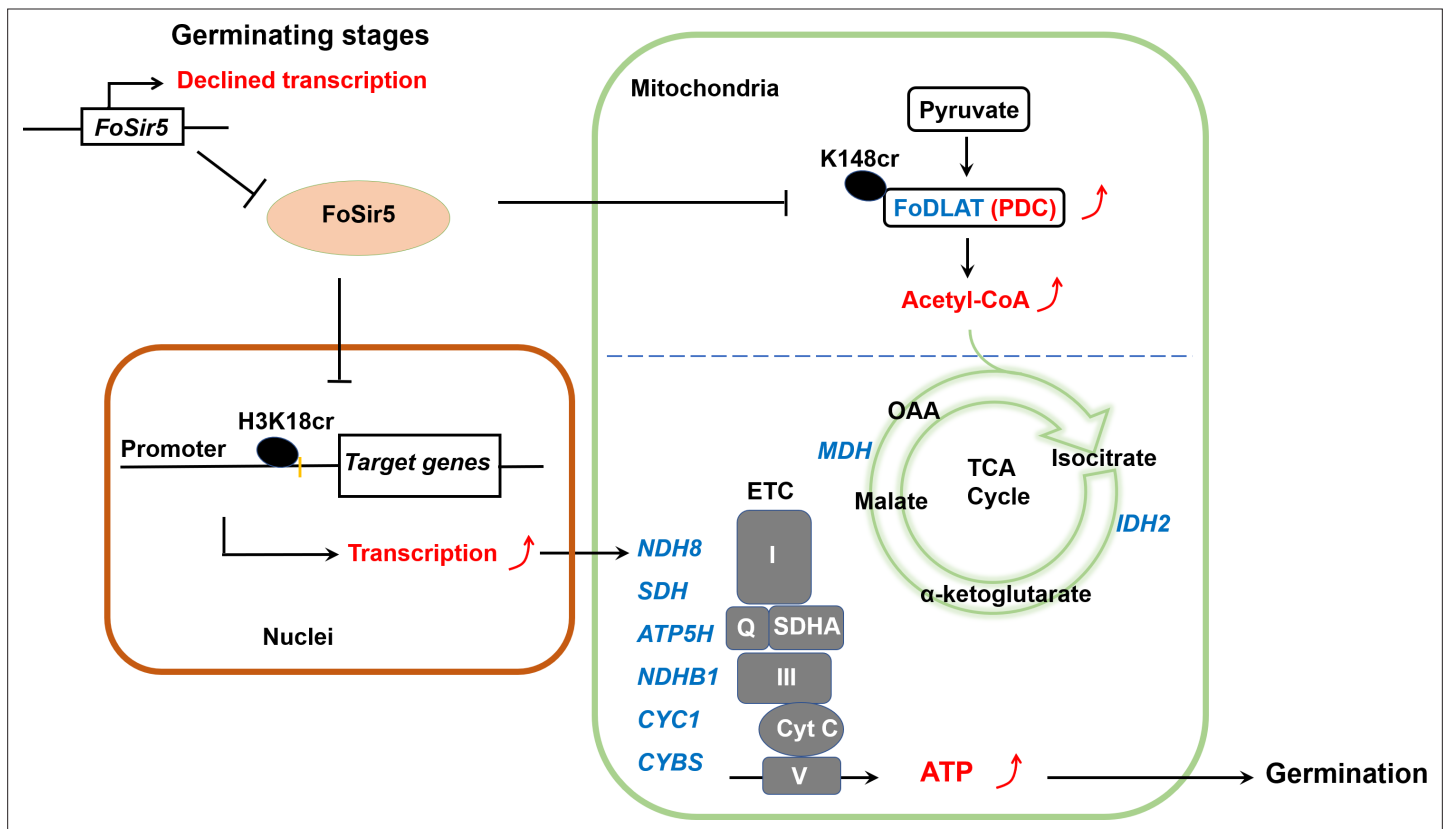


**Figure 6.** A model for FoSir5 functioning as a decrotonylase in different organelles to regulate conidial germination. During the germination process, the expression of *FoSir5* decreases, leading to relief of the inhibitory effect of FoSir5 on pyruvate dehydrogenase complex (PDC) activity through the decrotonylation of FoDLAT-K148cr and transcription of aerobic respiration-related genes by the reversal of H3K18cr. Thus, mitochondrial ATP biosynthesis is enhanced, promoting conidial germination in *Fusarium oxysporum*.